



ANALYTICAL METHODS TO ASSESS THE COLLAPSE AND DAMAGE OF REINFORCED CONCRETE WALLS

R. Jünemann⁽¹⁾, J.C. de la Llera⁽²⁾, M.A. Hube⁽³⁾.

⁽¹⁾ Assistant Professor, Department of Structural and Geotechnical Engineering and National Research Center for Integrated Natural Disaster Management CONICYT/FONDAP/15110017, Pontificia Universidad Católica de Chile, rjunemann@ing.puc.cl

⁽²⁾ Professor, Department of Structural and Geotechnical Engineering and National Research Center for Integrated Natural Disaster Management CONICYT/FONDAP/15110017, Pontificia Universidad Católica de Chile, jllera@ing.puc.cl

⁽³⁾ Associate Professor, Department of Structural and Geotechnical Engineering and National Research Center for Integrated Natural Disaster Management CONICYT/FONDAP/15110017, Pontificia Universidad Católica de Chile, mhube@ing.puc.cl

Abstract

During the great 2010, Chile earthquake, reinforced concrete (RC) buildings showed adequate performance. However, in some of them a particular damage pattern involving brittle failure of RC walls was observed in the lower stories, usually associated with high axial loads and vertical irregularities. The brittle nature of the failure led to a sudden degradation of the bending capacity and lateral stiffness of the walls. Significant research including experimental campaigns and numerical models has been conducted in order to describe the observed damage in RC walls and identify the possible causes of this behavior. This research studies the collapse and damage of shear wall buildings during the Maule earthquake using state-of-the-art analytical models. The proposed analytical research lies within the family of micro models, and uses finite element models with 4-node shell elements to represent the physical interactions that occur in the wall section at finite element level. Inelastic finite element models were developed in DIANA, and the concrete was modeled following the *total strain rotating crack* approach. First, different stress-strain constitutive relationships for concrete in compression were evaluated and validated with experimental data. The stress-strain constitutive laws were regularized by preserving the compressive fracture energy, for both, unconfined and confined concrete. Once the constitutive models were validated, a real RC resisting plane damaged during the 2010, Chile earthquake was studied in detail, and the observed damage pattern reproduced by means of two-dimensional inelastic pushover analysis. It can be shown that the damage geometry of the shear wall cannot be correctly represented by conventional inelastic models that ignore the true deformation kinematics with lateral and axial interaction. Indeed, the failure mechanism of resisting planes shows strong coupling between lateral and vertical deformations in the plane. Finally, results of a three-dimensional inelastic dynamic analysis of the entire building are presented, which show to be consistent with the observed damage after the earthquake and with the 2D model results.

Keywords: shear wall damage, pushover analysis, inelastic finite element models, dynamic inelastic analysis, reinforced concrete buildings, thin shear walls.



1. Introduction

The typical Chilean RC building characterizes by rely almost exclusively on a system of RC shear walls to withstand gravity and lateral loads, with a floor plan configuration with a central longitudinal corridor with RC walls in the transverse direction, so they are called “fish-bone” RC buildings. Wall densities range most commonly between 1.5% to 3.5% in each direction, with a mean value of 2.8%, a characteristic that has remained almost constant in time [1][2][3] and has been historically considered as the responsible of the good seismic behavior of this type of buildings during the 1985 Chile earthquake [4][5].

Although in general terms this type of structures also performed well during the large 2010 Chile earthquake ($M_w=8.8$), extensive localized brittle damage occurred in some of these structures located in the cities of Santiago, Viña del Mar and Concepción. Observed damage was typically concentrated in first story and basements, and it was characterized by concrete crushing over a short height. In several cases, this damage was spread almost over the entire length of the wall. Reinforcement buckling and fracture was observed, and global wall buckling was also found in some cases. Different authors have reported detailed descriptions of observed damage after 2010 earthquake in RC wall buildings [6][7][8][9][10]. Damaged buildings were in a large majority modern buildings constructed after year 2000, characterized by small wall thickness, high axial loads, and vertical irregularities [11]. However, many buildings of similar topology did not undergo damage during the earthquake.

Research on the brittle failure observed in RC walls has been mainly focused on analytical and experimental work on isolated RC wall specimens. For RC walls with high axial load ratios combined with poor confinement, as was the case of Chilean buildings, damage have shown to be localized in a reduced region of the wall, characterized by an abrupt flexural-compressive failure just after spalling of concrete cover, as shown by Alarcon *et al.*[12]. Furthermore, Massone *et al.* [13] and Arteta *et al.* [14], tested RC boundary elements with different levels of confinement under pure compression. On the one hand, Massone *et al.* [13] showed that although confinement traduces in a more ductile response, it is less effective in thinner specimens, thus a greater thickness is required to properly confine a boundary element. On the other hand, Arteta *et al.* [14] proved experimentally that more confinement could not prevent a brittle behavior of boundary elements when subjected to pure compression.

Different analytical tools have been used in the past to represent the behavior of RC walls, which can be grouped in micro-modeling and macro-modeling. Micro-modeling discretize the walls into small elements where concrete and steel are considered separately, such as finite element models or fiber element models. In macro-models, the overall behavior of a RC wall is represented as a whole [15]. Specifically for Chilean RC walls, Magna *et al.* [16][16] have used a multi-spring macro-model including a horizontal shear spring with calibrated properties. Also, Vasquez *et al.* [17] have proposed a new force-based fiber element (FFE) for cyclic analysis including shear effects, buckling, and fracture of steel bars.

Regarding finite element models, two main approaches are commonly considered to model concrete fracture: the *cohesive crack* model, which assumes the fracture localized in a discrete crack, and the *smearred crack* model, which assumes that fracture is distributed within a continuum with a defined stress-strain relationship. Within the *smearred crack* model, a *decomposed strain* concept or a *total strain* concept can be considered for the stress-strain relations. In the first case the strain is decomposed into elastic (ϵ_e) and cracking (ϵ_{cr}) strain components, while in the second case the stress is considered as a function of the total strain. Additionally, there are two alternatives to model the shear stress-strain relationships: *fixed* and *rotating*. In the *fixed crack* model the principal axes are fixed during the post-cracking phase, while in the *rotating crack* model the principal axes co-rotate with the principal strains during crack propagation [18]. The smeared crack model has been widely used in finite element models and has been implemented in different available software [19]. The *total strain rotating crack* model implemented in the software DIANA [20] allows for orthotropic material and has been used by other authors showing good results to represent RC behavior [21][22][23].

This article aims to reproduce the observed damage in RC walls after 2010 Chile earthquake by means of inelastic finite element models using DIANA, and to identify critical modeling assumptions. First, different stress-strain constitutive models of concrete were evaluated and validated with experimental data for both confined and



unconfined concrete. Second, a RC resisting plane of a test-bed building damaged during the 2010 Chile earthquake was studied in detail by means of two-dimensional pushover analysis. In the pushover analysis, concrete was modeled by the *smearred cracking* approach, while reinforcement was modeled using an embedded formulation, which assumes perfect bonding. Despite these model limitations, it is shown that the 2D pushover models provide useful information that helps understand the rupture mechanism that occurred in these walls. Finally, a three-dimensional finite element model of the entire building is presented, where the inelastic behavior is concentrated in the first story and basements. Results from dynamic inelastic analysis are consistent with the damage observed in the building after 2010 earthquake.

2. Inelastic finite element model for RC walls

Inelastic finite element models presented herein are developed in DIANA [20] using the *total strain rotating crack* model. Concrete is modeled using the Q8MEM element, which is a four-node quadrilateral iso-parametric plane stress element, with linear interpolation displacement field, and Gauss-point integration quadrature. Different constitutive models were evaluated to simulate the inelastic behavior of concrete in compression: (i) constant (CONS), which depends only on the concrete compressive strength f'_c and the young modulus E_c ; (ii) Thorenfeldt (THOR), which is function of the unit-dependent parameters n and k that can be assumed by the software [20] or provided by the user ; (iii) Parabolic (PARA), which is based on the compressive fracture energy G_c , and the crack bandwidth h , which is related to the element size; and (iv) Multilinear (MULT), which is based on a user defined set of stress-strain lines. Additionally, three concrete behavior effects are included according to the software available options: increase of strength due to lateral confinement; compression softening effect; and decrease in Poisson's ratio with increased cracking. For tensile behavior, Hordijk constitutive model is used, which is based on the tensile strength f_t , the tensile fracture energy G_f , and the crack bandwidth. CEB-FIP (1990) [24] code recommendations are considered to estimate tensile properties, i.e. $f_t = 1.4(f'_c/f'_{c0})^{2/3}$ and $G_f = G_{f0}(f'_c/f'_{c0})^{0.7}$, where f'_c is the concrete compressive strength, $f'_{c0} = 10$ MPa, and $G_{f0} = 0.058$ MPa-mm [24].

In order to minimize the mesh-size effects, an energy regularization method is applied to the concrete stress-strain relations with strain-softening. For the PARA model, the software automatically modifies the stress-strain relationship based on the element size. For THOR and MULT models, the respective parameters of the stress-strain relation are adjusted in order to keep the compressive fracture energy G_c constant, i.e., $G_c = h \int_{\epsilon_0}^{\epsilon_u} \sigma(\epsilon) d\epsilon$ (Fig.1(a)), where h is the crack bandwidth. The compressive fracture energy is assumed as an inherent material property and can be estimated as $G_c = 8.8 \sqrt{f'_c}$ for plain concrete following recommendations by Nakamura and Higai [25].

In order to estimate the compressive fracture energy for confined concrete, an element of equivalent size $h_{eq} = \frac{G_{uc}}{\int_{\epsilon_0}^{\epsilon_u} \sigma_{uc}(\epsilon) d\epsilon}$ is considered, where $\sigma_{uc}(\epsilon)$ is the stress-strain constitutive relationship, and $G_{uc} = 8.8 \sqrt{f'_c}$ is the compressive fracture energy, both for unconfined concrete. Then, the compressive fracture energy for confined concrete G_{cc} is estimated as $G_{cc} = h_{eq} \int_{\epsilon_0}^{\epsilon_u} \sigma_{cc}(\epsilon) d\epsilon$, where $\sigma_{cc}(\epsilon)$ is the stress-strain constitutive relationship for confined concrete. In this case, the stress-strain constitutive models proposed by Karthik and Mander [26], and by Kent and Park [27][27], are analyzed and the average fracture energy obtained by considering both constitutive models is considered.

Reinforcement is modeled using the BAR element, based on an embedded formulation assuming perfect bonding [20]. An exponential hardening rule is considered for both tension and compression, neglecting bar fracture in tension and/or buckling in compression. This is a limitation of the proposed model, as bar buckling was observed in damaged walls after the 2010 earthquake.

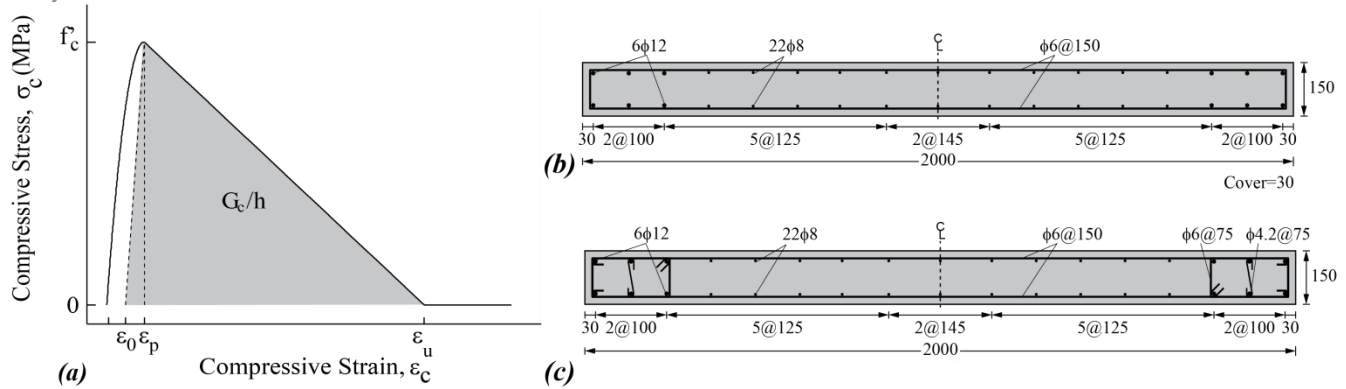


Fig. 1 – a) stress-strain relation for concrete in compression; b) unconfined rectangular specimen (WSH4); and c) confined rectangular specimen (WSH3).

The finite element model and regularization technique are validated with the test results of two walls tested by Dazio *et al.* [28]. The rectangular walls WSH4 and WSH3 are considered, which were subjected to lateral cyclic displacement. The height of the walls was 456 cm, and they were tested under an axial load ratio (ALR) of 6%, which is calculated as the total axial load relative to $A_g f'_c$ and expressed in percentage. The geometry of the specimens is shown in Fig.1(c) and (d) and the material properties are summarized in Table 1, where tensile properties f_t and G_f have been estimated according to CEB-FIP (1990) [24] recommendations, G_{uc} has been estimated according to Nakamura and Higai [25], and G_{uc} has been estimated according to the previously described methodology. The rest of the material properties are the mean values obtained from tests [28].

Table 1 – Material properties of selected RC wall specimens.

ID	Concrete					Steel		
	f'_c (MPa)	E (MPa)	G_{uc} (MPa-mm)	G_{cc} (MPa-mm)	f_t (MPa)	G_f (MPa-mm)	f_y (MPa)	C (MPa)
WSH4	41	38,500	56.3	-	3.58	0.155	576	98.9
WSH3	39	35,200	55.1	308.9	3.48	0.151	601	124.5

For the unconfined specimen (WSH4), four different mesh sizes were used to validate the proposed regularization methodology, $h=20, 10, 5$ and 2.5 cm. Fig.2(a) shows schematically the wall model, where the displacements in the base nodes are constrained. Vertical load is applied as a first load case, and lateral displacement is applied gradually in the nodes located at the horizontal actuator height as a second load case. The four different concrete stress-strain constitutive models considered in compression (CONS, THOR, (PARA, and MULT), are shown in Fig.2(b), after energy regularization is applied.

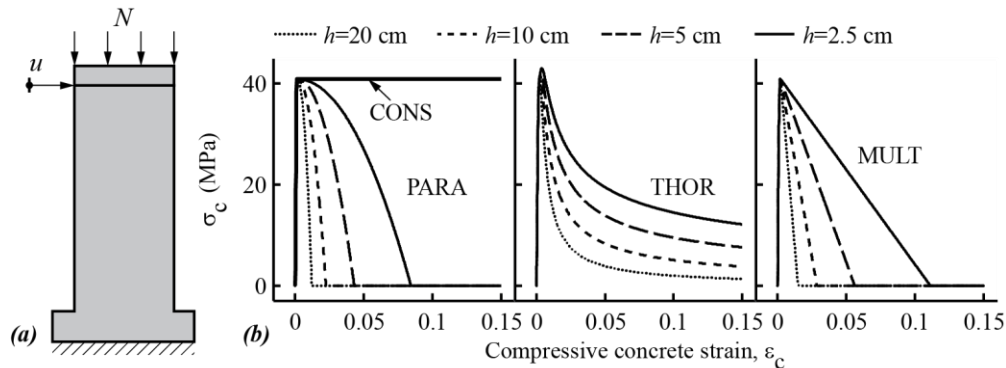


Fig. 2 – a) Schematic view of the wall model; and b) compression stress-strain for PARA, THOR and MULT models, respectively and for different mesh sizes.

Force-displacement results for wall WSH4 are shown in Fig.3(a) through 3(d) for the different constitutive models for concrete in compression and for the different mesh sizes. Results show that in general, all models provide a good estimate of the strength of the specimen. Table 2 presents a summary of the strength obtained with each model and mesh-size. The measured strength during the test was $V_n=433$ ton. The strength predicted by each model and the difference between the experimental and analytical strengths are summarized in Table 2, where ΔF_{mesh} and ΔF_{model} correspond to the maximum difference for each row or column, respectively. On the one hand, the effect of the mesh-size for a given constitutive model (ΔF_{mesh} in Table 2) is small, varying between 3% and 11%. Model CONS is the one that presents the smaller difference with the experimental measurements, followed by PARA and MULT models, while THOR model presents the largest difference. On the other hand, the effect of the constitutive model for a given mesh size (ΔF_{model}) varies between 6% and 11%; therefore, all models provide in this case a good estimation of the experimental lateral strength of the specimen.

Table 2 – Maximum strength estimated by finite element models relative to the measured strength ($V_n = 443$ ton).

σ - ϵ Model	Maximum Strength (kN)				ΔF_{mesh}
	Mesh size h				
	0.2	0.1	0.05	0.025	
CONS	441	430	428	438	3%
PARA	422	420	425	434	5%
THOR	403	395	400	417	11%
MULT	420	420	428	439	5%
ΔF_{model}	9%	11%	10%	6%	

Regarding the ultimate behavior estimated by the analytical models, Fig.3(a) shows that CONS model completely misses the ultimate behavior of the wall WSH4, while the other constitutive models (Fig.3(b)-(d)) present better results. Apparently MULT model is the best model in predicting the ultimate behavior of the specimen for all mesh sizes, but PARA model also gives good results, with the advantage that no manual regularization is required, which is relevant for finite element models with elements of different sizes.

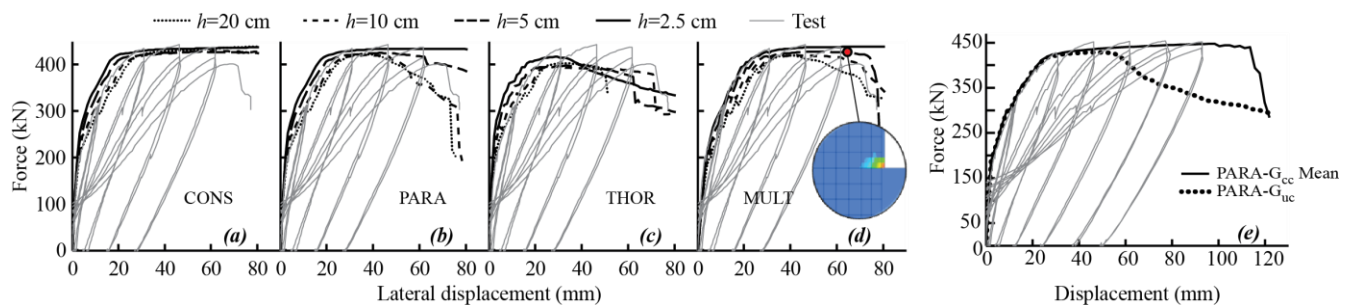


Fig. 3 – Force vs top displacements results: a) Specimen WSH4, CONS model; b) specimen WSH4, PARA model; c) specimen WSH4, THOR model; d) specimen WSH4, MULT model; and e) specimen WSH3, PARA model.

Wall WSH3 is a rectangular specimen with the same layout as wall WSH4, but with confined boundary elements as shown in Fig.1(c). The average confined compressive fracture energy estimated in this case is $G_{cc} = 308.1$ MPa-mm, as presented in Table 1. Fig.3(e) shows results for the finite element model using a mesh-size $h=10$ cm and the PARA model considering: (i) unconfined (G_{uc}) for all elements (PARA- G_{uc}); and (ii) mean confined fracture energy (G_{cc}) for the boundaries and unconfined fracture energy (G_{uc}) for the rest of the wall (PARA- G_{cc} Mean). It is apparent that using unconfined concrete properties G_{uc} for all concrete elements is not adequate as the wall capacity is underestimated. However, using mean confined concrete fracture energy G_{cc} at boundary elements gives reasonable results, which validates the proposed model for confined concrete.

4. Pushover analysis of a damaged RC wall

The analytical model described earlier is applied to a resisting plane that was severely damaged during the 2010 earthquake. The selected resisting plane, called herein wall Q, is part of a RC wall building located in Santiago, with 18 stories and 2 basements and a “fish-bone” like configuration (Fig.4). The building has an average wall thickness of 20 cm, an average shear wall density (total area of walls divided by tower area, calculated at the first level above grade) of 6.5%, and a fundamental period of 0.86 s in the N-S direction, which was estimated from an ETABS model of the building.

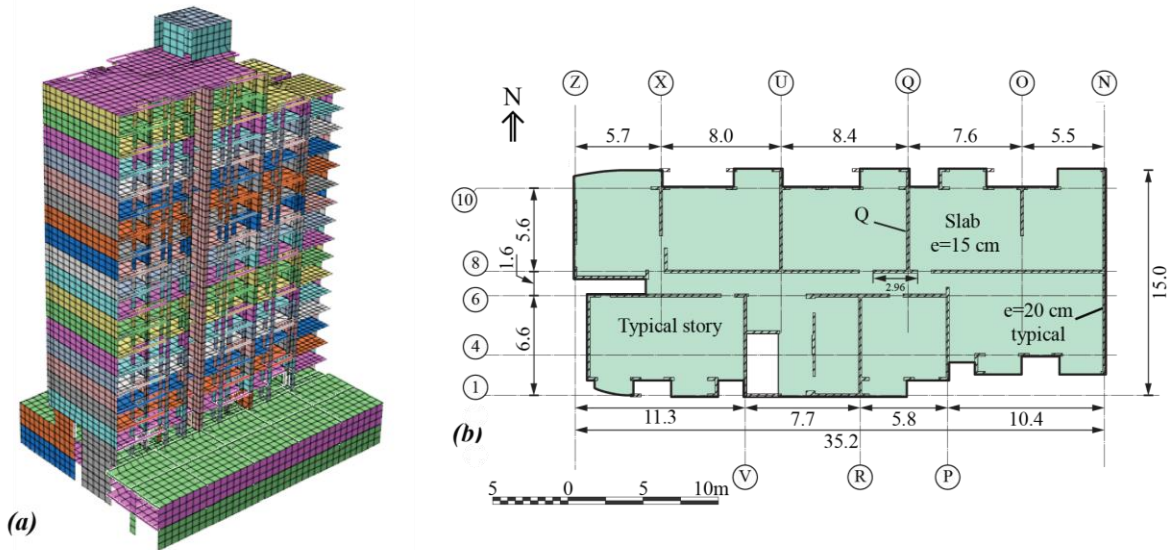


Fig. 4 – a) Finite element model of the building (for dynamic analysis); and b) typical story floor plan.

Wall Q is a flag-shaped transverse wall with orientation N-S characterized by a significant irregularity in the transition from basements to first story, where the wall changes in length and cross-section, as shown in Fig.5(a), (b) and (c). The wall suffered extensive damage during the earthquake, which concentrated in the first basement, as shown in Fig.5(d). The damage was characterized by concrete crushing over almost the entire length of the wall. Similar damage was observed also in other resisting planes of the same building (axis U and N, Fig.4(b)) while moderate damage was observed in other walls located also in the north-side of the building [29]. No significant damage was reported on RC slabs and other RC walls.

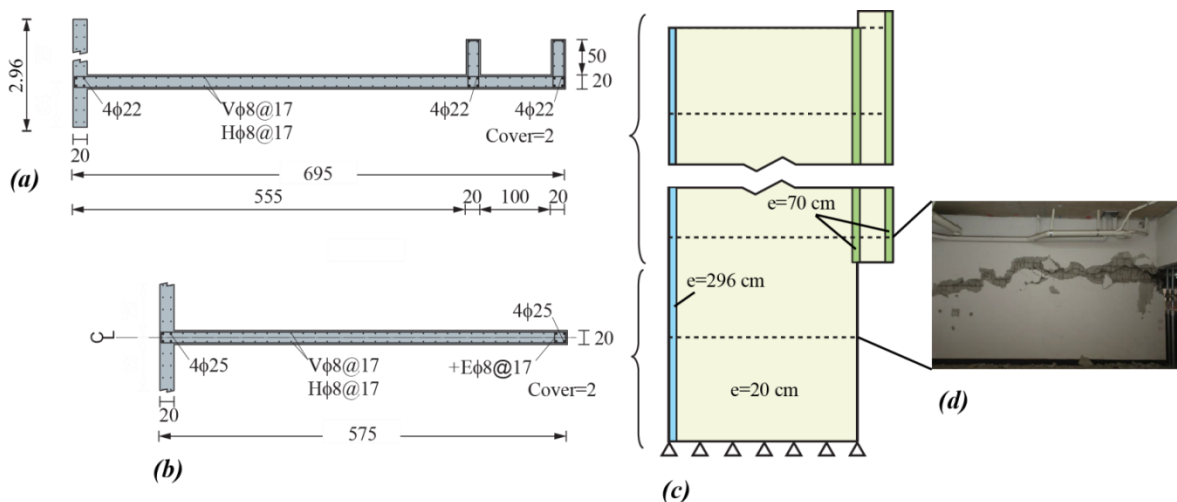


Fig. 5 – Wall Q: a) cross section from first story and up; b) cross section at basements; c) schematic model elevation; and d) observed damage after 2010 earthquake.

Fig.5(c) schematically shows the model layout for the pushover analysis of wall Q, where the web of the shear wall is modeled using 20 cm thick shell elements, the wall flange (axis 8, Fig.4(b)) is modeled using 296 cm thick shell elements according to the dimension of the flange from first story and up (Fig.5(a)), and the orthogonal wall segments in the opposite side of the wall are modeled with 70 cm thick shell elements. Horizontal and vertical displacements are restricted at the base nodes (second basement), and gravitational loads (dead loads plus 25% live loads) are obtained from a 3D linear finite element model of the building and applied to the nodes at each floor level of the wall model. The finite elements are 10 cm side, and the PARA constitutive model was used to model concrete compressive behavior. Unconfined compressive fracture energy was considered, since the confinement of the wall is very limited.

For the pushover analysis, four different displacement patterns or load cases were imposed into the wall, as schematically shown in Fig.6(a). First, case R corresponds to a constant lateral displacement at all roof nodes of the wall. Second, case T corresponds to floor lateral nodal displacements that increase in height according to an inverted triangular pattern. Third, case M1 corresponds to floor lateral nodal displacements that result from the predominant elastic mode shape in the direction of the wall. Finally, case MV1 corresponds to floor lateral and vertical nodal displacements that result from the predominant elastic mode shape. The vertical displacements included in the last load case aim to represent the 3D interaction between the wall and the rest of the surrounding structure, in order to capture variations in the axial load of the wall due to lateral motion of the building.

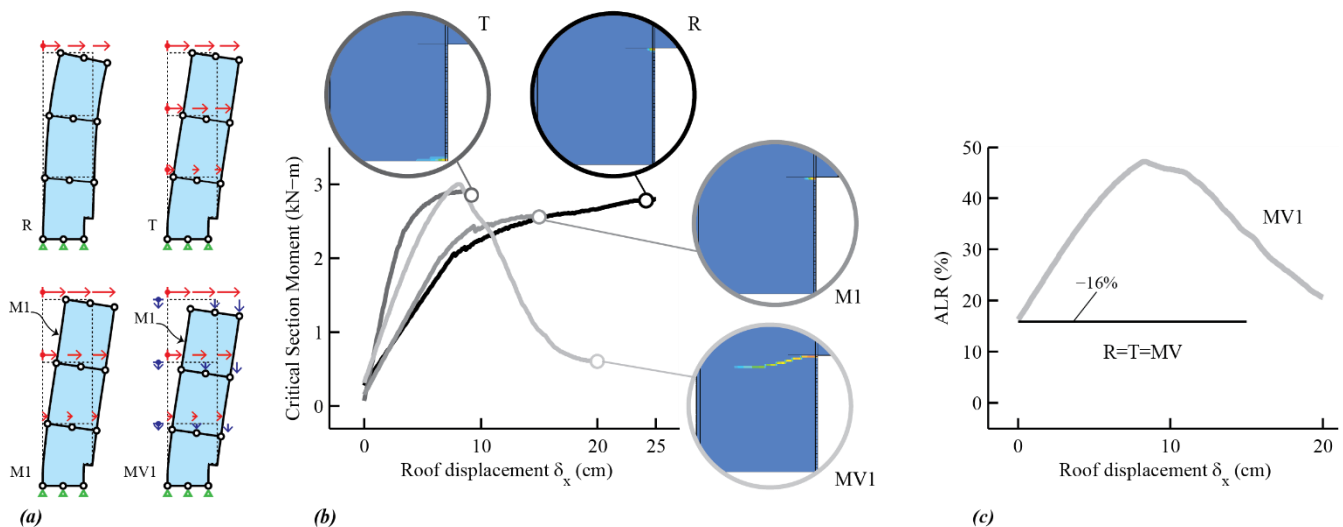


Fig. 6 – a) Pushover displacement patterns; b) moment-displacement results for the different load cases; and c) ALR results for the different load cases.

Fig.6(b) shows the bending moment at the critical section of the wall versus the roof displacement and the concrete plastic deformations of the bottom of the wall for the four displacement patterns considered in the pushover analysis. The critical section of the wall corresponds to the first basement, below the vertical irregularity. The first three displacement patterns (R, T, M1) implicitly assume a constant axial load in the wall, which is equal to the gravity load, i.e. ALR=16%, as shown in Fig.6(c). This effect translates into rather poor predictions of the damage pattern for the wall, which are not consistent with the horizontal crack observed after the earthquake (Fig. 5(d)). On the one hand, patterns R and M1 do not show strength degradation and although the plastic deformations are concentrated at the irregularity between the basement and first story, crushing does not propagate toward the interior of the wall and these displacement patterns fail to reproduce the observed damage after the earthquake. On the other hand, pattern T predicts a limited ductility behavior, but damage localizes at the bottom of the wall and does not reproduce the observed damage pattern. Finally, case MV1 presents clear strength degradation after the roof displacement exceeds approximately 9 cm, and resembles the observed damage pattern after the earthquake. A maximum ALR of 47% is obtained for case MV1 (Fig.6(c)), which is more consistent with the expected dynamic amplification factors due to seismic actions [11].

4. Dynamic inelastic analysis of a damaged building

This section presents a finite element model of the entire building using the software DIANA [20], where the inelastic material behavior was modeled as described in the previous section using PARA constitutive model for concrete in compression. The finite element model is shown in Fig. 4(a). The damage after 2010 earthquake was concentrated mainly in walls located at the first basement, and no significant damage was reported on other stories nor in the slabs. Therefore, the inelastic behavior of the finite element model is concentrated in all vertical elements at the first three levels of the building (Fig.7), with the exception of perimeter walls at the basements. The rest of the building was modeled with linear elastic behavior.

In general, walls and slabs were modeled using three or four node triangular or quadrilateral iso-parametric curved shell elements with five degrees of freedom per node (three translations and two rotations), based on linear interpolation and 2x2 Gauss integration scheme over the element area. Beams were modeled with frame elements. Basement levels were included in the model and all nodes at the base were restricted from lateral and vertical displacements. No rigid diaphragms were included at floor levels and the effect of surrounding soil at the basements was neglected. The self-mass of the structural elements corresponding to the dead loads plus 25% of the live loads was included in the model. Damping was included through Rayleigh damping with 3% damping at 1.2 times the first elastic period and at the elastic period for which the mass participation factor was more than 75% in both principal directions. The model was subjected to the different components of the ground motion recorded in the nearby station Peñalolen [30]. A brittle compressive failure consistent with the damage observed after the earthquake was predicted by the model for when the critical component of the seismic record was applied to the N-S direction of the building [29].

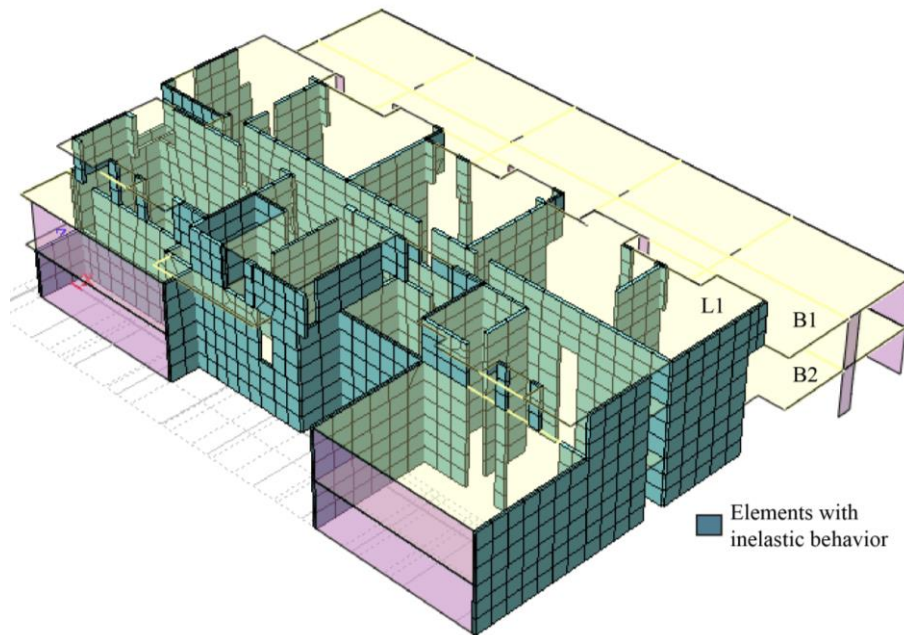


Fig. 7 – Three-dimensional inelastic finite element model, first three levels.

Shown in Figures 8 and 9 are the local response obtained for the critical section of wall Q. First, Fig.8(a) shows the concrete stress-strain relationship in the vertical direction of the critical integration point of element 1 (Fig.8(c)), where it is clear that the strain corresponding to peak compressive stress is exceeded, and the stress drops to zero. Fig.8(b) shows the history of vertical concrete strains for one integration point of each of the five finite elements shown in Fig.8(c). At 71.8 s, concrete strains increase dramatically in more than one finite element, reaching values higher than 0.5%, which implies concrete crushing and damage of the wall. No significant inelastic incursion of any element is observed before this time, with the exception of concrete cracking. Fig.9(a) shows the ALR history at the critical section of wall Q, where at the failure instant ($t=71.8$ s), the maximum compressive

ALR is 35%. Additionally, the bending moment history at the critical section is shown in Fig.9(b), and the concrete plastic strains are shown in Fig.9(c) for the instant just after the failure ($t=71.8$ s). From this results it is concluded that the failure predicted by the finite element model resembles the damage pattern observed after the earthquake (Fig.5(d)), as significant compressive strains are predicted along the entire length of the wall at the critical section. Additionally, the model predicts an abrupt failure as it occurs within one cycle. The failure is predicted for an ALR=35%, which corresponds to a dynamic amplification factor of 2.2 with respect to the gravity condition (ALR=16%).

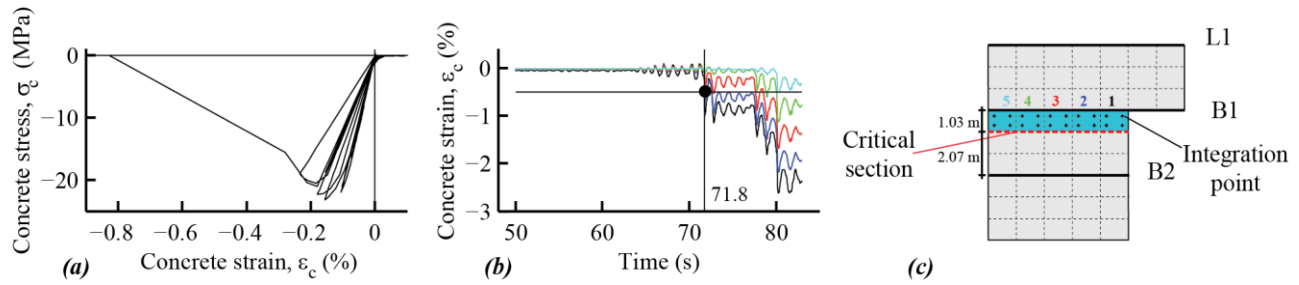


Fig. 8 – Local response for wall Q: a) stress-strain behavior for the critical integration point; b) concrete strains for the critical elements; c) scheme of critical section and integration points of the wall.

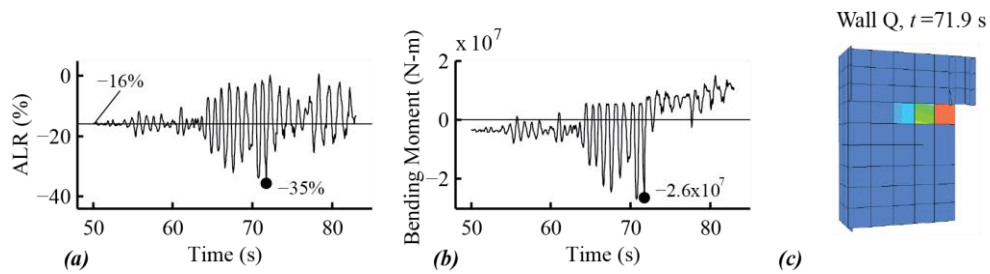


Fig. 9 – Local response for wall Q: a) ALR at critical section history; b) bending moment at critical section history; c) concrete crushing in the critical section.

The kinematic of wall Q at the failure instant predicted by the inelastic model is compared with the kinematic of the wall according to the first elastic mode of the building, both scaled to the same lateral roof displacement (Fig.10). It is apparent that both kinematics are consistent, thus, using the first elastic mode shape to evaluate the 2D response of this type of walls through a pushover analysis may be a good proxy to the inelastic response, as presented elsewhere [31][31].

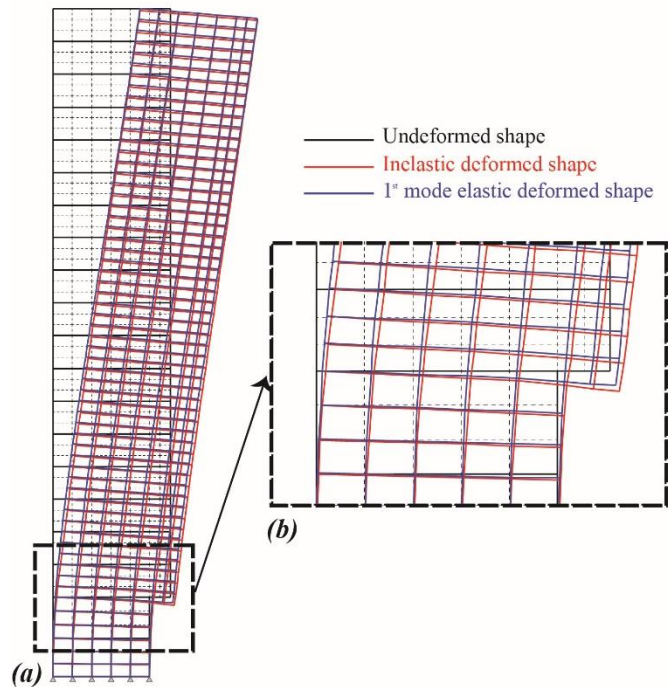


Fig. 10 – Local response for wall Q: a) undeformed and deformed shape; b) zoom of undeformed and deformed shape.

5. Discussion and conclusions

This article explores the use of inelastic finite element models in DIANA to assess the earthquake damage in RC wall buildings. First, different stress-strain constitutive relationships for concrete in compression were evaluated and validated with experimental data. Then, inelastic pushover analysis of a RC wall damaged during 2010 Chile earthquake was developed. It is concluded that the damage predicted by the model showed good agreement with the damage observed after the earthquake when a load displacement pattern that includes lateral and vertical displacements according to the first elastic mode of the building is considered (MV1). The model predicts low ductility behavior with a failure localized in the first basement, just below the vertical irregularity of the wall, which propagates to the interior of the web of the wall. The failure is associated with a large increase in the axial load ratio in the wall, which is consistent with the physically expected behavior. Results show that the displacement patterns that only consider lateral displacements (R, T, and M1) are unable to reproduce the damage pattern observed in the wall during the earthquake. These models completely miss the effect of axial load increase due to the 3D interaction between the wall and the rest of the structure.

Additionally, results of a dynamic inelastic analysis of a 3D finite element model of the entire building are presented. The model considers the inelastic material behavior concentrated in the first three levels of the building, while the rest of the structure was modeled linear elastic. This model also predicts an abrupt compressive failure in the wall consistent with the observed damage after the earthquake. Results show almost no inelastic excursion prior to failure, and again, a significant increase in the axial load ratio of the wall. Additionally, the kinematic of the first elastic building mode seems to be a good proxy of the kinematic condition of the inelastic dynamic analysis at the instant of failure. Although the ALR predicted by the 3D dynamic inelastic analysis (ALR=35%) is lower than the one predicted by the load case MV1 in the pushover analysis (ALR=47%), the latter load case seems to be a good proxy for predicting the wall behavior using a 2D pushover analysis.

Although the models presented in this article have evident limitations, the model results presented herein consistently show that the wall behavior was brittle, and hence, concrete compressive strains increased dramatically within one cycle, causing a sudden loss in wall capacity at instants with high ALRs. Furthermore, the wall response is strongly affected by the 3D interaction within the building and the distribution of the walls in plan



by inducing a significant increase in ALR. Thus, the use of an isolated cantilever wall, commonly assumed in design, would not be consistent with the behavior estimated by the analytical models. Although our evidence does not show it, it is impossible to rule out completely that the wall damage could have been produced by a different mechanism associated with lighter axial loads and degradation due to cyclic behavior.

4. Acknowledgements

This research has been sponsored by the National Science and Technology Council of Chile, CONICYT, under grant Fondecyt 1141187, and by the National Research Center for Integrated Natural Disaster Management CONICYT/FONDAP/15110017. The authors are grateful for this support and would like to thank also the company Spöerer Ingenieros Asociados SpA.

5. References

- [1] Calderón JA. (2007) "Update on structural system characteristics used in RC building construction in Chile." Civil Engineering Thesis. University of Chile. p. 76 [in Spanish].
- [2] Gómez, C.E. (2001). Caracterización de Sistemas Estructurales Usados en las Viviendas de Hormigón Armado y Albañilería en Chile, Memoria para optar al título de Ingeniero Civil, Universidad de Chile.
- [3] Guzmán, M.A., (1998). Caracterización de Tipologías Estructurales Usadas en el Diseño de Edificios Altos en Chile, Memoria para optar al título de Ingeniero Civil, Universidad de Chile.
- [4] Wood SL. (1985). "Performance of reinforced concrete buildings during the 1985 Chile earthquake: implications for the design of structural walls." *Earthquake Spectra*; 7(4):607–638.
- [5] Hidalgo, P., Ledezma, C., Jordán, R., (2002). "Seismic Behavior of Squat Reinforced Concrete Shear Walls." *Earthquake Spectra*, 18(2):287-308.
- [6] Rojas F, Naeim F, Lew M, Carpenter LD, Youssef NF, Saragoni GR, Schachter M. (2011) "Performance of tall buildings in Concepcion during the 27 February 2010 moment magnitude 8.8 offshore Maule, Chile earthquake." *Structural Design of Tall and Special Buildings*; 20:37–64.
- [7] Carpenter LD, Naeim F, Lew M, Youssef NF, Rojas F, Saragoni GR, Schachter M. (2011) "Performance of tall buildings in Viña del mar during the 27 February 2010 offshore Maule, Chile earthquake." *Structural Design of Tall and Special Buildings*; 20:17–36.
- [8] Westenenk B, de la Llera JC, Besa JJ, Jünemann R, Moehle J, Lüders C, Inaudi JA, Elwood KJ, Hwang S-J. (2012) "Response of reinforced concrete buildings in Concepción during the Maule earthquake." *Earthquake Spectra*; 28(S1):S257–80.
- [9] Westenenk B, de la Llera JC, Jünemann R, Hube MA, Besa JJ, Lüders C, Inaudi JA, Riddell R, Jordán R. (2013) "Analysis and interpretation of the seismic response of RC buildings in Concepción during the February 27, 2010 Chile Earthquake." *Bulletin of Earthquake Engineering*; 11(1):69–91.
- [10] Wallace JW, Massone LM, Bonelli P, Dragovich J, Lagos R, Lüders C, Moehle J. Damage and Implications for Seismic Design of RC Structural Wall Buildings. *Earthquake Spectra* 2012; 28(S1); S281-S299.
- [11] Jünemann R., de la Llera J.C., Hube M.A., Cifuentes L.A., Kausel E. (2015) "A statistical analysis of reinforced concrete wall buildings damaged during the 2010, Chile earthquake". *Engineering Structures*, 82 (2015) 168–185.
- [12] Alarcon C., Hube M.A., de la Llera J.C. (2014) "Influence of axial load in the seismic behavior of RC walls unconfined wall boundaries." *Engineering Structures*; 73:13-23.
- [13] Massone L.M., Polanco P., Herrera P. (2014) "Experimental and analytical response of RC wall boundary elements" *Proceedings of the 10th National Conference in Earthquake Engineering*, Earthquake Engineering Research Institute, Anchorage, AK.
- [14] Arteta C.A., To D.V., Moehle J.P. (2014) "Experimental response of boundary elements of code-compliant reinforced concrete shear walls." *Proceedings of the 10th National Conference in Earthquake Engineering*, Earthquake Eng. Research Institute, Anchorage, AK.
- [15] Galal K., El-Sokkary H. (2008) Advancement in modeling of RC shear walls." *Proceedings of the 14th World Conference on Earthquake Engineering*, Beijing, China



- [16] Magna-Verdugo C.E., Kunnath S.K. (2014) "Non-linear response analysis of reinforced concrete shear walls using multi-spring macro-models." Proceedings of the 10th National Conference in Earthquake Engineering, Earthquake Engineering Research Institute, Anchorage, AK.
- [17] Vasquez J.A., de la Llera J.C., Hube M.A. (2015) "A regularized fiber element model for reinforced concrete shear walls". Earthquake Engineering and Structural Dynamics, accepted for publication.
- [18] Feenstra P.H., de Borst R., and Rots J.G. (1991) "A comparison of different crack models applied to plain and reinforced concrete." Proceedings of the International RILEM/ESIS Conference "Fracture Processes in Concrete, Rock and Ceramics", Noordwijk, The Netherlands.
- [19] Johnson A. (2006) "Comparison of Nonlinear Finite Element Modeling Tools for Structural Concrete". CEE561 Project, University of Illinois
- [20] TNO DIANA. (2010). DIANA - User's Manual.
- [21] Hube M.A. and Mosalam K.M. (2011). "Experimental and computational evaluation of in-span hinges in reinforced concrete box-girder bridges." Journal of Structural Engineering, Vol. 137, No. 11, pp. 1245-1253.
- [22] Quiral F. (2013) "Non-linear brittle behavior of shear wall buildings during 2010 Chile earthquake." Master of Science Thesis. Pontificia Universidad Católica de Chile. (in Spanish)
- [23] Dashti F., Dakhil R.P., and Pampanin S. "Numerical simulation of shear wall failure mechanisms", Proceedings of the New Zealand Society for Earthquake Engineering 2014 Conference, Auckland, New Zealand.
- [24] Comité Euro-International du Béton. (1990). CEB-FIP model code 1990, Thomas Telford, London.
- [25] Nakamura, H., & Higai, T. (2001). "Compressive fracture energy and fracture zone length of concrete." Modeling of Inelastic Behavior of RC Structures under Seismic Loads, p471-487.
- [26] Karthik M., Mander J. "Stress-block parameters for unconfined and confined concrete based on a unified stress-strain model." Journal of Structural Engineering 2011; 137 (2):270-273.
- [27] Scott, B., Park, R., & Priestley, M. (1982). "Stress-strain behavior of concrete confined by overlapping hoops at low and high strain rates." ACI Journal Proceedings, (79), 13-27.
- [28] Dazio A., Beyer K., and Bachmann H. (2009) "Quasi-static cyclic tests and plastic hinge analysis of RC structural walls." Engineering Structures; 31:1556-1571
- [29] Jünemann R., (2016) Response of Reinforced Concrete Shear Wall Buildings during 2010 Chile Earthquake. PhD Thesis, Pontificia Universidad Católica de Chile
- [30] Universidad de Chile. Departamento de Ingeniería Civil and Oficina Nacional de Emergencia Chile (ONEMI). Earthquakes of Chile; 2010. <<http://terremotos.ing.uchile.cl/2010>> [in Spanish] [accessed 11.05.16].
- [31] Jünemann R., de la Llera J.C., Hube M.A., Vasquez J.A., Chacón M.F. (2016) "Study of the damage of reinforced concrete shear walls during the 2010, Chile earthquake", Earthquake Engineering and Structural Dynamics; 45(10): 1621-1641